Available online at www.sciencedirect.com
SCIENCE DIRECT®
International Journal of Heat and Mass Transfer 47 (2004) 1989–1996
International Journal of HEAT and MASS TRANSFER
www.elsevier.com/locate/ijhmt

Non-isothermal flow of a polymeric liquid passing an asymmetrically confined cylinder

Y.M. Lin [a], G.H. Wu [a,*], S.H. Ju [b]

[a] Department of Mechanical Engineering, National Cheng-Kung University, Tainan, Taiwan 701, ROC
[b] Department of Civil Engineering, National Cheng-Kung University, Tainan, Taiwan 701, ROC

Received 10 April 2003

Abstract

Non-isothermal polymeric flow past an asymmetrically confined cylinder has been analyzed using a finite-element based numerical technique. The fluid model in this numerical simulation is a differential-type non-isothermal Bird–Carreau model describing the non-Newtonian behavior of the melt. The generated thermal field is entirely due to viscous heating. Drag, lift force and heat transfer on the cylinder and other flow characteristics are predicted. The influences of cylinder lateral position and Reynolds number are also investigated.

1. Introduction

The flow of a polymeric liquid past a cylinder between plates has been a research topic of considerable interest in recent years. Non-Newtonian effects, such as shear-thinning, temperature-thinning and inertia, that possessed by most polymeric liquids are significant in these flow situations. The understanding of such flow is required for important engineering applications and has attracted a great deal of attention in the literature.

Several researchers have studied flow past a symmetrically confined cylinder both experimentally and numerically. Dhahir and Walters [1] measured the force on a cylinder placed in a channel flow. They report that viscoelasticity results in drag reduction. McKinley [2] used LDV (laser doppler velocimetry) to measure the flow around a cylinder fixed in the middle of a channel. A downstream shift in the streamlines was reported. Calculations were conducted for non-isothermal flow, by Wu [3] using EVSS finite-element methodology. They found that non-isothermal drag is lower than isothermal drag, and is more significant at higher Reynolds numbers.

In the case of an asymmetrically confined cylinder, a lateral force arises and tends to push the cylinder towards the closer wall. Dhahir and Walters [1] measured also the force on an asymmetrically-placed cylinder in a channel flow, and found that viscoelastic increase results in increased lateral force but reduced drag on the cylinder. These results were corroborated by the numerical simulations of Carew and Townsend [4]. Cochrane [5] observed that streak lines are much more sensitive to small asymmetry in cylinder confinement in a viscoelastic fluid than in a purely viscous Newtonian fluid.

It is well known that the influences of temperature change are often very important in polymer processing. In this paper, we shall study non-isothermal effects on polymeric flow past an asymmetrically confined cylinder by numerical simulations using a finite-element method. The generated thermal field is entirely due to viscous heating. Drag force, lift force and heat transfer on the cylinder and other flow characteristics are predicted. The influences of cylinder lateral position and Reynolds number are also examined.

2. Mathematical modelling

Fig. 1 describes the geometry of the present problem, i.e. non-isothermal flow of a shear-thinning and

* Corresponding author. Tel.: +886-6-2757575x62179; fax: +886-6-2208643.
E-mail address: d1014519@mail.ncku.edu.tw (G.H. Wu).

0017-9310/$ - see front matter © 2003 Elsevier Ltd. All rights reserved.
doi:10.1016/S0017-9310(03)00349-1

Nomenclature

Br	Brinkman number
C_p	Specific heat capacity, kJ/kg °C
$\boldsymbol{d}$	rate-of-deformation tensor, s^{-1}
k	thermal conductivity, W/m K
Nu	Nusselt number
p	pressure, N/m^2
Pe	Peclet number
Re	Reynolds number
R	ideal gas constant, J/mole K
d	diameter of the cylinder, m
U	mean velocity, m/s
T^*	dimensionless temperature

Greek symbols

∇	gradient operator, m^{-1}
ρ	free stream density, kg/m^3
ε	eccentricity factor
$\boldsymbol{\tau}$	shear-stress tensor, N/m^2
$\dot{\boldsymbol{\gamma}}$	shear-rate tensor, s^{-1}
$\langle\dot{\gamma}\rangle$	average shear-rate, s^{-1}
$\eta(\dot{\gamma}, T)$	viscosity function, Pa s
ϕ_i	quadratic basic function
ψ_i	bilinear basic function

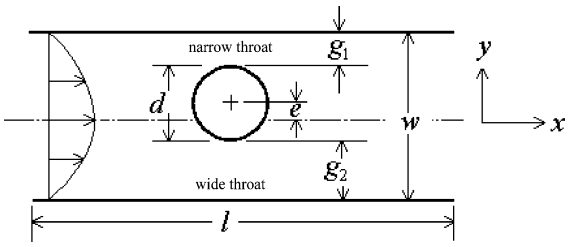

Fig. 1. Geometry of the channel flow past an asymmetrically confined cylinder.

temperature-thinning polymeric fluid, low-density polyethylene (LDPE), through a channel with an asymmetrically confined cylinder. Refered to Fig. 1, channel dimensions are $h = 14$ mm and $l = 400$ mm; cylinder diameter $d = 4$ mm. The laternal position of the cylinder is indicated by an eccentricity factor

$$\varepsilon = e/(h/2 - d/2). \tag{1}$$

Thus $\varepsilon = 0$ when the cylinder sits on the centerline of the channel; $\varepsilon = 1$ when the cylinder touches the wall.

Non-isothermal flow of a polymeric fluid is governed by the following set of conservation and constitutive equations.

Continuity equation:

$$\nabla \cdot \boldsymbol{v} = 0 \tag{2}$$

Momentum equation, neglecting body forces:

$$\rho(\boldsymbol{v} \cdot \nabla)\boldsymbol{v} = -\nabla p + \nabla \cdot \boldsymbol{\tau} \tag{3}$$

where $\boldsymbol{\tau}$ is the extra stress.

The total stress tensor is expressed as

$$\boldsymbol{\sigma} = -p\boldsymbol{I} + \boldsymbol{\tau} \tag{4}$$

where p is pressure and $\boldsymbol{I}$ is the unit tensor.

Table 1
Rheological data and material functions used in the non-isothermal Bird–Carreau model for LDPE

$\eta = \eta(\dot{\gamma}, T) = \eta_0(T)[1 + (\lambda\dot{\gamma})^2]^{(n-1)/2}$	$\rho = 900\ \mathrm{kg\,m^{-3}}$
$\eta_0(T) = \eta_{0,\mathrm{ref}} \exp\left[\frac{E}{R}(1/T - 1/T_{\mathrm{ref}})\right]$	$C_p = 1535\ \mathrm{J\,kg^{-1}\,K^{-1}}$
$\eta_0(T_w) = \eta_{0,\mathrm{ref}} = 19\,500$ Pa s	$k = 0.329\ \mathrm{W\,m^{-1}\,K^{-1}}$
$E = 11\,700$ cal/mol K	$R = 8.3$ J/(mole K)
$n = 0.52$	$T_w = 433$ K
$\lambda = 5.5$ s	$T_{\mathrm{ref}} = 433$ K

For fluids with constant properties: density ρ, heat capacity C_p, and thermal conductivity k, the energy equation is given as

$$\rho C_p \boldsymbol{v} \cdot \nabla T = \nabla \cdot k(\nabla T) + \boldsymbol{\tau} : \boldsymbol{d} \tag{5}$$

where $\boldsymbol{d} = (\nabla \boldsymbol{v} + \nabla \boldsymbol{v}^{\mathrm{T}})/2$.

The generalized-Newtonian fluid model used by [6] to model the non-isothermal flow of a LDPE melt is defined by the following equation, together with the curved-fitted parameters and material functions in Table 1:

$$\boldsymbol{\tau} = 2\eta\boldsymbol{d} \tag{6}$$

where viscosity function $\eta = \eta(\dot{\gamma}, T)$ is temperature and shear-rate dependent. The shear-rate dependence is described by the Carreau model, while the temperature dependence is of the Arrhenius type.

Velocity is considered to be fully developed isothermally at the inlet. No slip boundary condition is applied at the wall. Wall temperature is constant throughout. Inlet temperature is assumed equal to wall temperature. At the outlet, zero normal-force and zero heat-flux are assumed.

3. Numerical method

The Galerkin finite-element method [7] is used to solve the present flow problem and applied as follows.

3.1. Dimensionless governing equations

By applying the transformations $\boldsymbol{v}^* = \boldsymbol{v}/U$, $\nabla^* = h\nabla$, $\eta^* = \eta/\eta_{0,\mathrm{ref}}$, $T^* = (T - T_\mathrm{w})/(T_\mathrm{b} - T_\mathrm{w})$, $p^* = ph/U\eta_{0,\mathrm{ref}}$, and $\boldsymbol{\tau} = \tau h/U\eta_{0,\mathrm{ref}}$ to Eqs. (2)–(6), the dimensionless governing equations are obtained:

$$\nabla^* \cdot \boldsymbol{v}^* = 0 \tag{7}$$

$$Re\,\boldsymbol{v}^* \cdot \nabla^* \boldsymbol{v}^* = \nabla^* \cdot (-p^* \boldsymbol{I} + \boldsymbol{\tau}^*) \tag{8}$$

$$Pe\,\boldsymbol{v}^* \cdot \nabla^* T^* = \nabla^{*2} T^* + Br\,\boldsymbol{\tau}^* : \boldsymbol{d}^* \tag{9}$$

In these equations, Reynolds, Peclet and Brinkman numbers are defined respectively as:

$$Re = \rho U h/\eta_{0,\mathrm{ref}} \tag{10}$$

$$Pe = \rho C_p h U/k \tag{11}$$

$$Br = \eta_{0,\mathrm{ref}} U^2/k(T_\mathrm{b} - T_\mathrm{w}) \tag{12}$$

where $\eta_{0,\mathrm{ref}}$ is viscosity at both zero shear-rate and the reference temperature, and T_b is defined as $T_\mathrm{b} = T_\mathrm{w} + 1(K)$.

3.2. Weak formulation of dimensionless governing equations

The field variables are interpolated within each element by

$$\boldsymbol{v}^* = \sum_{i=1}^{N=8} \phi_i \boldsymbol{v}_i^*, \quad p^* = \sum_{i=1}^{M=4} \psi_i p_i^*, \quad T^* = \sum_{i=1}^{N=8} \phi_i T_i^*$$

where $\boldsymbol{v}_i^*$, p_i^*, T_i^* are nodal values and ϕ_i, ψ_i are quadratic and bi-linear basic functions, respectively.

Following traditional Galerkin manipulation, the weak form of the dimensionless governing Eqs. (7) and (8) can be derived as:

$$\int_\Omega \psi_i (\nabla^* \cdot \boldsymbol{v}^*)\,\mathrm{d}\Omega = 0 \tag{13}$$

$$\int_\Omega [\phi_i'(Re\,\boldsymbol{v}^* \cdot \nabla^* \boldsymbol{v}^*) + \nabla^* \phi_i' \cdot (-p^* \boldsymbol{I} + \boldsymbol{\tau}^*)]\,\mathrm{d}\Omega - \int_s \phi_i \boldsymbol{n} \cdot (-p^* \boldsymbol{I} + \boldsymbol{\tau}^*)\,\mathrm{d}s = 0 \tag{14}$$

where $\phi_i' = \phi_i + (\tilde{\boldsymbol{k}}^* \boldsymbol{v}^*/\boldsymbol{v}^* \cdot \boldsymbol{v}^*) \cdot \nabla^* \phi_i$.

The traditional Galerkin method is known to be inappropriate when the convective terms in the energy equation become dominant as the Peclet number increases. The streamline-upwind/Petrov–Galerkin formulation (SUPG) developed by Brooks and Hughes [8] is used to suppress undesirable oscillations in the calculation of the temperature fields. To solve the equation by this method, an additional weighing function formulation $(\tilde{\boldsymbol{k}}^* \boldsymbol{v}^*/\boldsymbol{v}^* \cdot \boldsymbol{v}^*) \cdot \nabla^* \phi_i$ is applied to all terms of the energy Eq. (5), where $\tilde{\boldsymbol{k}}^*$ is the dimensionless form of $\tilde{\boldsymbol{k}}$ proposed by Brooks and Hughes. Consequently, the following weak forms are finally obtained:

$$\int_\Omega \{\phi_i'[Pe\,\boldsymbol{v}^* \cdot \nabla^* T^* - Br\,\boldsymbol{\tau}^* : \boldsymbol{d}^*] + \nabla^* \phi_i' \cdot \nabla^* T^*\}\,\mathrm{d}\Omega - \int_s \phi_i \boldsymbol{n} \cdot \nabla^* T^*\,\mathrm{d}s = 0 \tag{15}$$

Since the integrals in Eqs. (13)–(15) are integrals of polynomial functions, they may be readily evaluated numerically using Gaussian quadrature. The above discretization processes lead to a system of non-linear equations of the form

$$K(x^*)x^* = f^* \tag{16}$$

where $\boldsymbol{K}(\boldsymbol{x}^*)$ is global stiffness matrices, $\boldsymbol{f}^*$ is the force vector, $\boldsymbol{x}^* = v_x^{*(1)} \cdots v_x^{*(n_1)}, v_y^{*(1)} \cdots v_y^{*(n_1)}, \quad p^{*(1)} \cdots p^{*(n_2)}, T^{*(1)} \cdots T^{*(n_3)}$, and n_1, n_2, n_3 are respectively the number of velocity, pressure and temperature nodal points.

The Newton–Raphson iteration method is employed to solve the above set of non-linear equations. Due to sparseness and asymmetry of the global stiffness matrix, the biconjugate gradient stabilized (BiCGStab) method [9] has been developed to compute all the unknowns at each iteration step. Convergence is considered to be achieved when the relative error of each of the dimensionless variables is less than 10^{-4}.

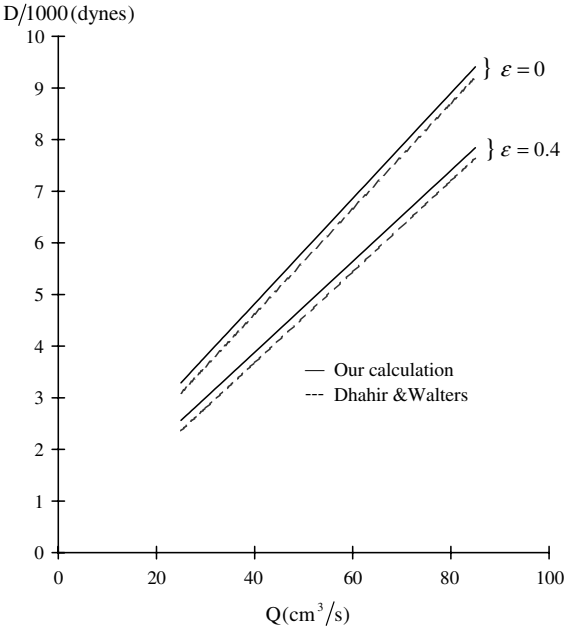

Fig. 2. Comparison between our numerical results and those of Dhahir and Walters [1].

4. Results and discussion

4.1. Test case

We have found no data in the literature that affords a complete check of the validity of our methodology. One previous study seems to serve this purpose to some extent. Dhahir and Walters [1] computed the force and torque on a cylinder fixed at different eccentric positions in a viscoelastic channel flow. They found the drag and lift force on the cylinder per unit length of the cylinder as

$$D = -\int_0^{2\pi} [\sigma_{xx}\cos\theta + \sigma_{xy}\sin\theta]_{r=R} R\,\mathrm{d}\theta \tag{17}$$

$$L = -\int_0^{2\pi} [\sigma_{yy}\sin\theta + \sigma_{xy}\cos\theta]_{r=R} R\,\mathrm{d}\theta \tag{18}$$

where $\sigma_{xx} = -p + \tau_{xx}$, $\sigma_{yy} = -p + \tau_{yy}$, and $\sigma_{xy} = \tau_{xy}$.

To partially validate our methodology, we performed numerical simulation for the Newtonian case using our proposed methodology and the geometric parameters used by Dhahir and Walters, i.e. $h = 50$ mm, $l = 800$ mm and cylinder diameter $d = 30$ mm, as shown in Fig. 1. Our results are compared with those of Dhahir and Walters [1] in Fig. 2. As can be seen, the corresponding solutions are quite consistent.

4.2. Numerical simulation of non-isothermal flow of LDPE fluid passing an asymmetrically confined cylinder

Results for our present problem of non-isothermal flow of LDPE past a asymmetrically confined cylinder are presented now. Fluid properties are fixed, while flow-rate and lateral position of the cylinder are allowed to vary. Simulations are performed for a cylinder eccentricity factor ranging from 0 to 0.36 and a Reynolds number ranging from 0 to 0.000152, corresponding to a Peclet number ranging from 0 to 46 000.

An extensive mesh analysis to get a mesh-independent solution was first performed for the four eccentricity cases, $\varepsilon = 0$, 0.33, 0.50 and 0.66. This analysis gave four fine-enough finite-element meshes of 1736, 1612, 1550 and 1612 elements (labeled M1, M2, M3and M4, respectively) which are used for the computation, as

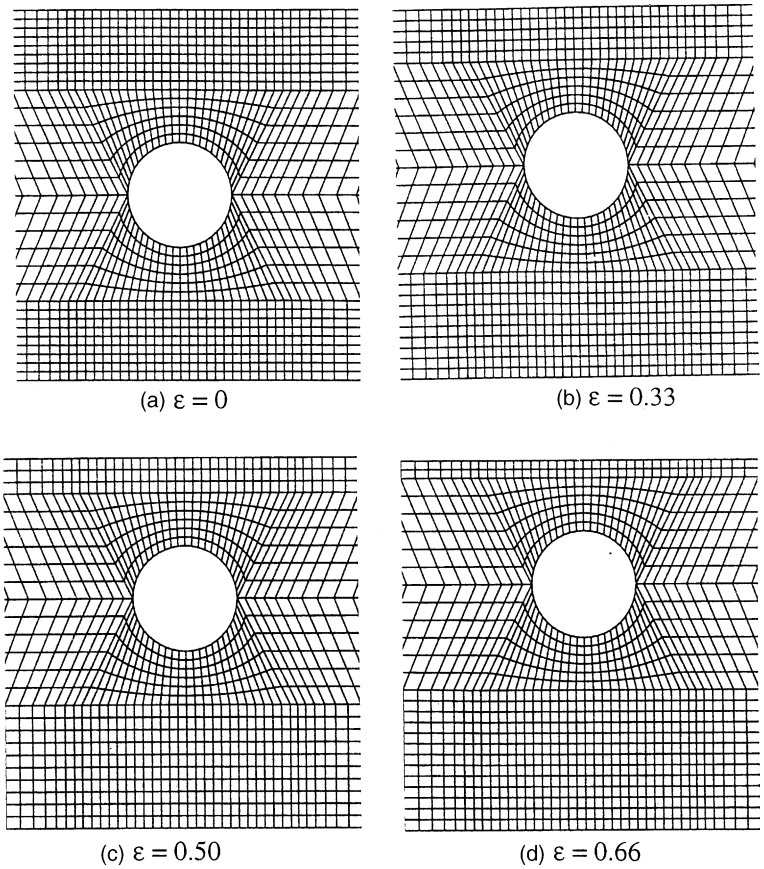

Fig. 3. Central portions of the finite element meshes used for the four eccentricity cases of $\varepsilon = 0$, 0.33, 0.50 and 0.66.

Table 2
Characteristics of the finite element meshes used

MESH	No. of elements	No. of nodes	No. of DOF
M1	1736	14 344	21 516
M2	1612	13 844	20 766
M3	1550	12 844	19 266
M4	1612	13 844	20 766

shown in Fig. 3. The number of nodes and degrees of freedom (DOF) associated with each mesh are summarized in Table 2.

The dimensionless temperature contours for the case of $\varepsilon = 0.50$ are shown in Fig. 4 for $Re = 0.000038$, 0.000076, and 0.000114. Because of the relatively large inlet width of the channel, heat dissipation is very small, and flow is close to being isothermal in the region upstream of the cylinder. However as the fluid passes through the throat (channel region with smallest distance between channel wall and cylinder) regions, it subjects to strong shear between cylinder and channel walls, results in sharp heat-dissipation and temperature rise in the near-wall regions. Dissipation heat is convected downstream, with maximum temperature occurring near the lower wall. The maximum temperature point moves downstream as flow-rate increases. For high Reynolds number ($Re > 0.00005$), i.e. high Peclet numbers, maximum temperature occurs at the outlet of the channel near the lower wall. Fig. 5 shows the variation of dimensionless maximum temperature T^*_{max} with eccentricity factor ε for four Reynolds numbers. It can be observed from Fig. 5 that T^*_{max} decreases with increasing ε in all cases. Moreover, downstream of the cylinder, temperature distribution near the lower wall is higher than near the upper wall, because the average velocity between the cylinder and the lower wall (wide throat) is larger between the cylinder and the upper wall

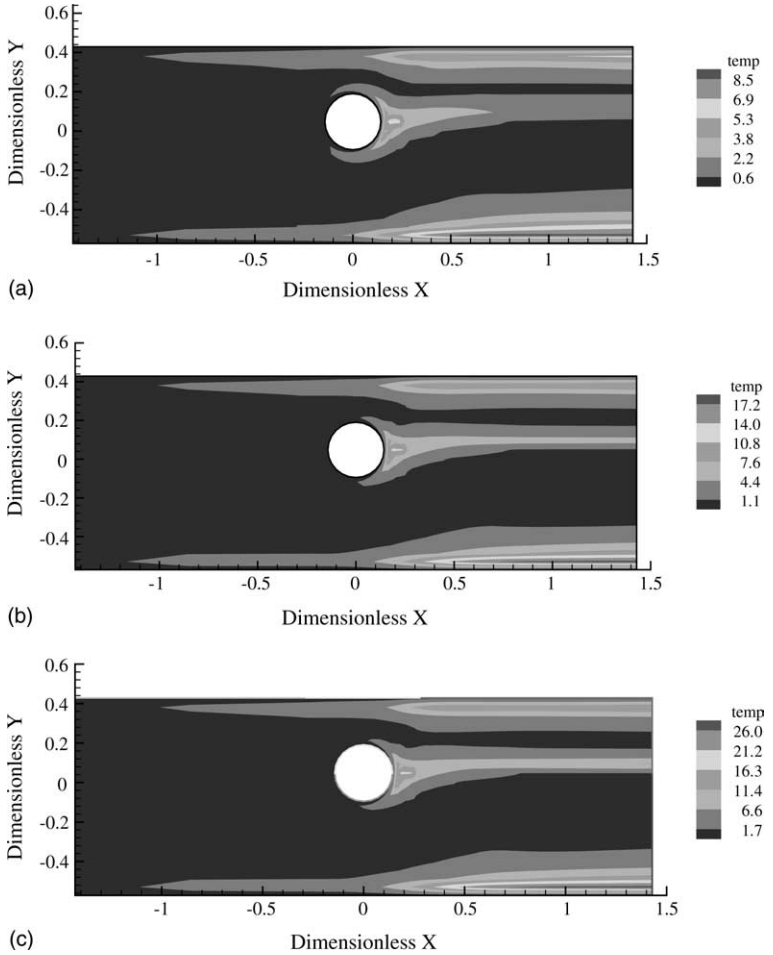

Fig. 4. Dimensionless temperature contours for the case of $\varepsilon = 0.50$ for three Reynolds numbers: (a) $Re = 0.000038$; (b) $Re = 0.000076$; (c) $Re = 0.000114$.

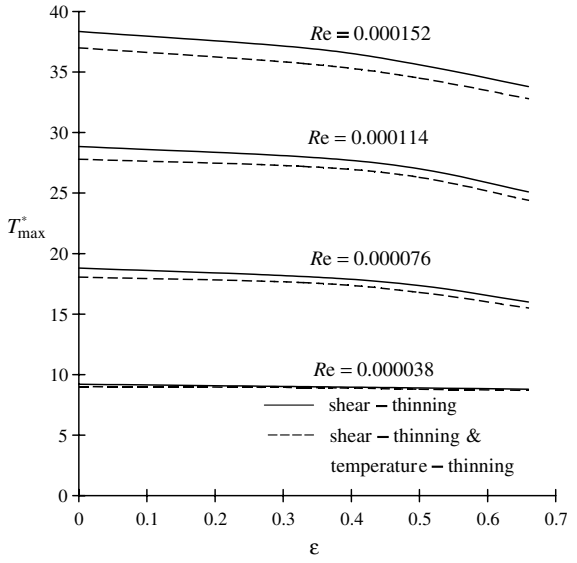

Fig. 5. T^*_{max} vs. ε for four values of Reynolds number.

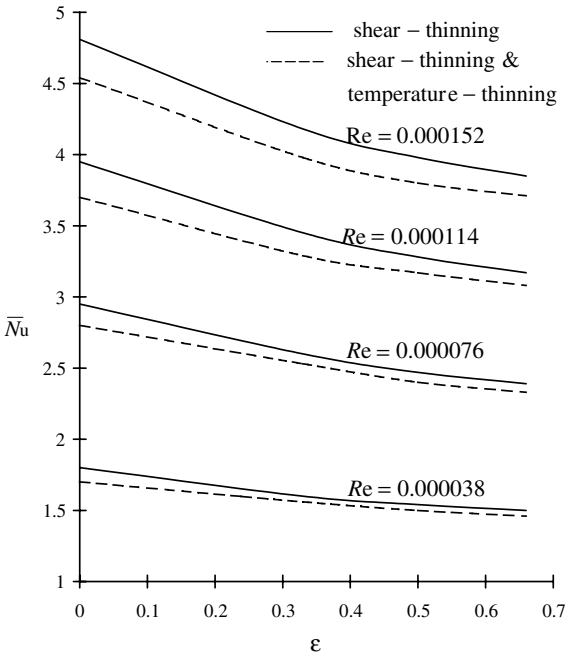

Fig. 6. $\overline{Nu}$ vs. ε for four Reynolds numbers.

(narrow throat). This is due to higher flow resistance occurring at the narrow throat.

4.2.1. Nusselt number

Local Nusselt number, Nu, and overall Nusselt number, $\overline{Nu}$, are defined by the following expressions, respectively, and can be readily derived from the temperature field of the numerical solutions:

$$Nu(\theta) = \left.\frac{\partial T^*}{\partial r^*}\right|_{r^*=1} \quad \text{and} \quad \overline{Nu} = \frac{1}{2\pi}\int_0^{2\pi} Nu(\theta)\,\mathrm{d}\theta \qquad (19)$$

$\overline{Nu}$ vs. eccentricity factor is shown in Fig. 6 for four Reynolds numbers. Due to the fact that a larger amount of heat is generated around the immersed cylinder with increased Reynolds number, $\overline{Nu}$ increases. For increased eccentricity, a lower $\overline{Nu}$ is predicted. Also, $\overline{Nu}$ decreases further when temperature-thinning property of the fluid is considered.

4.2.2. Drag on the cylinder

The drag and lift coefficients are defined as:

$$C_D = \frac{D}{(\rho U^2/2)d} \quad \text{and} \quad C_L = \frac{L}{(\rho U^2/2)d} \qquad (20)$$

where U is the mean velocity of the channel and d is the diameter of the cylinder.

Numerical solutions for D and L as a function of Re are plotted in Figs. 7 and 8, respectively, for three eccentricity cases. It is found that both D and L increase as Re increases for the above eccentricity cases. Figs. 9 and 10 show the variation of the above dimensionless

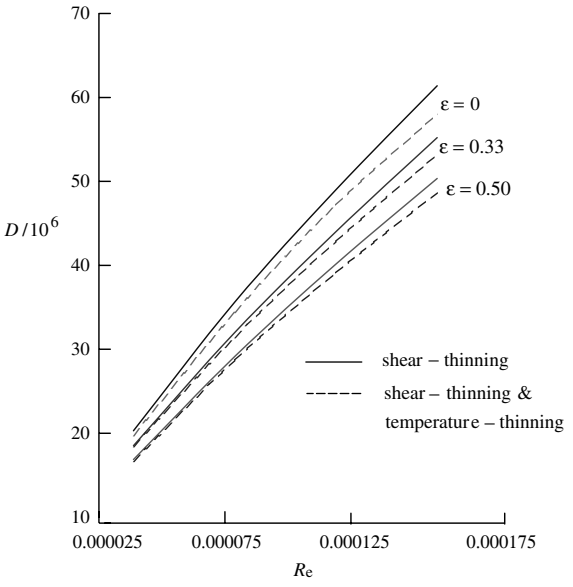

Fig. 7. D vs. Re for three eccentricity factors.

forces with Re for the three eccentricity cases. Decreased coefficients with Re are obtained. Furthermore, consideration of the temperature-thinning effect of the fluid reduces the above-calculated values C_D and D, but increases C_L and L.

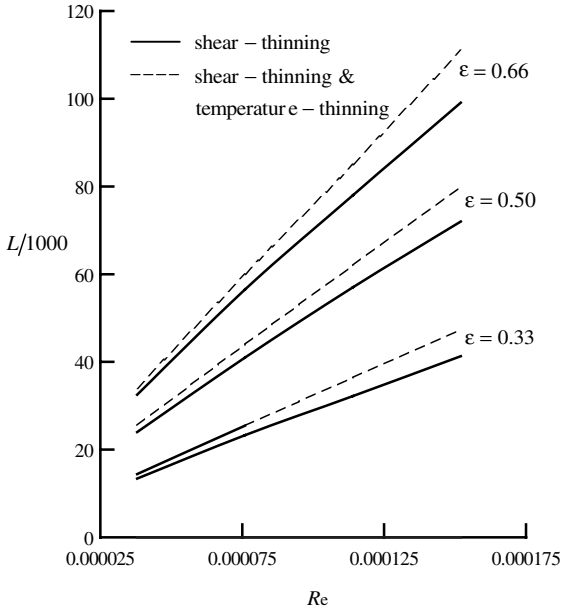

Fig. 8. L vs. Re for three eccentricity factors.

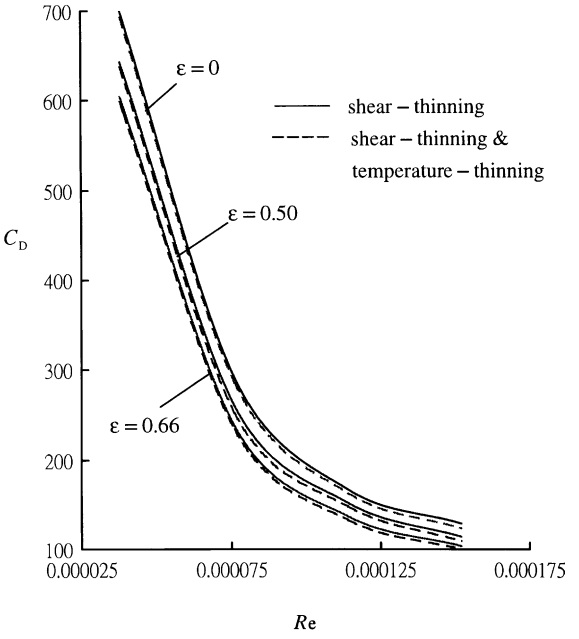

Fig. 9. C_D vs. Re for three eccentricity factors.

5. Conclusions

Non-isothermal polymeric flow past an asymmetrically-confined cylinder has been analyzed here using a finite-element based numeric technique. The generated thermal field is entirely due to viscous heating. It is found by the proposed simulation that:

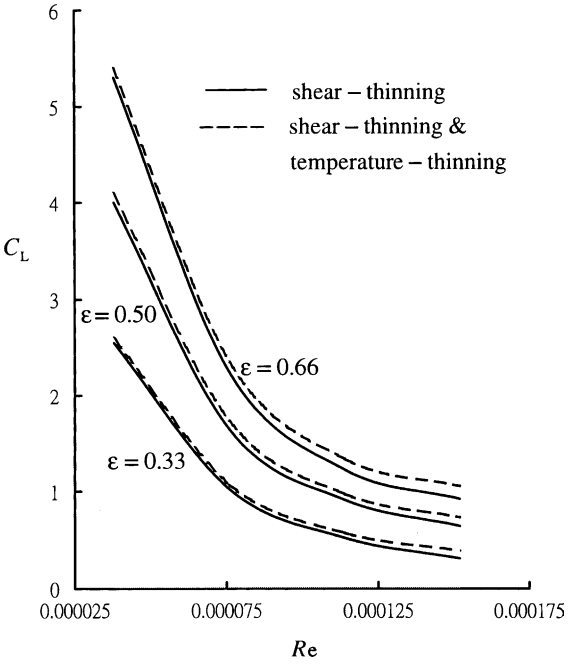

Fig. 10. C_L vs. Re for three eccentricity factors.

1. A high-temperature region downstream of the throat occurs as throat velocity gradient is significant.
2. Both drag and lift increase with increasing Reynolds number, but dimensionless drag and lift coefficients decrease.
3. When the cylinder gets close to the wall, drag on the cylinder decreases but lift increases.
4. Lift is very small compared with drag. If temperature-thinning property of the fluid is considered, drag decreases and lift increases.
5. $\overline{Nu}$ around the cylinder increases with increasing Reynolds number but decreases with increasing cylinder eccentricity, and decreases further if temperature-thinning property of the fluid is considered.
6. Maximum temperature occurs downstream of the wide throat in the near-wall region. As flow rate increases, this point moves further downstream. For high Peclet number ($Pe > 9000$), maximum temperature is predicted at the outlet near the wall of the wider throat. Maximum temperature difference between throat sides increases with increasing eccentricity.

References

[1] S.A. Dhahir, K. Walters, On non-Newtonian flow past a cylinder in a confined flow, J. Rheol. 33 (1989) 781–804.
[2] G.H. McKinley, Dynamics of polymer solutions, Ph.D. thesis, Massachusetts Institute of Technology, Cambridge, 1991.

[3] G.H. Wu, S.H. Ju, Numerical prediction of non-isothermal flow of nylon-6 past a cylinder between plates, J. Polym. Eng. 19 (4) (1999) 287–304.
[4] E. Carew, P. Townsend, Slow visco-elastic flow past a cylinder in a rectangular channel, Rheol. Acta 30 (1991) 58–64.
[5] T. Cochrane, K. Walters, M.F. Webster, On Newtonian and non-Newtonian flow in complex geometries, Philos. Trans. Roy. Soc. London, A 301 (1981) 163–181.
[6] M. Takase, R. Katsumoto, Numerical analysis of polymer melt flow in the nipping region, Polym. Eng. Sci. 42 (4) (2002) 836–845.
[7] V. Nassehi, Practical aspects of finite element modelling of polymer processingy, John Wiley, 2002.
[8] N. Brooks, T.J. Hughes, Steamline Upwind/Petrov-Galerkin ?tul> formulation for convection dominated flows with particular emphasis on the incompressible Navier–Stokes equations, Comp. Meth. Appl. Mech. Eng. 32 (1982) 199–259.
[9] H.A. VanDerVorst, BiCGSTAB: a fast and smoothly converging variant of Bi-CG for the solution of nonsymmetric linear system, SIAM, J. Sci. Atat. Comput. 13 (1992) 631–644.